

## Important Notice to Authors

Attached is a PDF proof of your forthcoming article in PRA. Your article has 5 pages and the Accession Code is **AY11417**.

Please note that as part of the production process, APS converts all articles, regardless of their original source, into standardized XML that in turn is used to create the PDF and online versions of the article as well as to populate third-party systems such as Portico, Crossref, and Web of Science. We share our authors' high expectations for the fidelity of the conversion into XML and for the accuracy and appearance of the final, formatted PDF. This process works exceptionally well for the vast majority of articles; however, please check carefully all key elements of your PDF proof, particularly any equations or tables.

Figures submitted electronically as separate PostScript files containing color appear in color in the online journal. However, all figures will appear as grayscale images in the print journal unless the color figure charges have been paid in advance, in accordance with our policy for color in print (<http://journals.aps.org/authors/color-figures-print>).

**No further publication processing will occur until we receive your response to this proof.**

### Specific Questions and Comments to Address for This Paper

- 1 Please update arXiv. Refs [23,27].
- 2 Please check updated journal information and check for correct page number.

Open Funder Registry: Information about an article's funding sources is now submitted to Crossref to help you comply with current or future funding agency mandates. Crossref's Open Funder Registry (<https://www.crossref.org/services/funder-registry/>) is the definitive registry of funding agencies. Please ensure that your acknowledgments include all sources of funding for your article following any requirements of your funding sources. Where possible, please include grant and award ids. Please carefully check the following funder information we have already extracted from your article and ensure its accuracy and completeness: National Research Foundation, Prime Minister's office (Singapore)

### Other Items to Check

- Please note that the original manuscript has been converted to XML prior to the creation of the PDF proof, as described above. Please carefully check all key elements of the paper, particularly the equations and tabular data.
- Title: Please check; be mindful that the title may have been changed during the peer review process.
- Author list: Please make sure all authors are presented, in the appropriate order, and that all names are spelled correctly.
- Please make sure you have inserted a byline footnote containing the email address for the corresponding author, if desired. Please note that this is not inserted automatically by this journal.
- Affiliations: Please check to be sure the institution names are spelled correctly and attributed to the appropriate author(s).
- Receipt date: Please confirm accuracy.
- Acknowledgments: Please be sure to appropriately acknowledge all funding sources.
- Hyphenation: Please note hyphens may have been inserted in word pairs that function as adjectives when they occur before a noun, as in "x-ray diffraction," "4-mm-long gas cell," and "R-matrix theory." However, hyphens are deleted from word pairs when they are not used as adjectives before nouns, as in "emission by x rays," "was 4 mm in length," and "the R matrix is tested."

Note also that Physical Review follows U.S. English guidelines in that hyphens are not used after prefixes or before suffixes: superresolution, quasiequilibrium, nanoprecipitates, resonancelike, clockwise.

- Please check that your figures are accurate and sized properly. Make sure all labeling is sufficiently legible. Figure quality in this proof is representative of the quality to be used in the online journal. To achieve manageable file size for online delivery, some compression and downsampling of figures may have occurred. Fine details may have become somewhat fuzzy, especially in color figures. The print journal uses files of higher resolution and therefore details may be sharper in print. Figures to be published in color online will appear in color on these proofs if viewed on a color monitor or printed on a color printer.
- Please check to ensure that reference titles are given as appropriate.
- Overall, please proofread the entire *formatted* article very carefully. The redlined PDF should be used as a guide to see changes that were made during copyediting. However, note that some changes to math and/or layout may not be indicated.

### Ways to Respond

- **Web:** If you accessed this proof online, follow the instructions on the web page to submit corrections.
- **Email:** Send corrections to [praproofs@aptaracorp.com](mailto:praproofs@aptaracorp.com)  
Subject: **AY11417** proof corrections
- **Fax:** Return this proof with corrections to +1.703.791.1217. Write **Attention:** PRA Project Manager and the Article ID, **AY11417**, on the proof copy unless it is already printed on your proof printout.

- **Mail:** Return this proof with corrections to **Attention:** PRA Project Manager, Physical Review A, c/o Aptara, 3110 Fairview Park Drive, Suite #900, Falls Church, VA 22042-4534, USA.

## Quantifying the role of thermal motion in free-space light-atom interaction

Yue-Sum Chin,<sup>1</sup> Matthias Steiner,<sup>1,2</sup> and Christian Kurtsiefer<sup>1,2,\*</sup>

<sup>1</sup>Center for Quantum Technologies, 3 Science Drive 2, Singapore 117543

<sup>2</sup>Department of Physics, National University of Singapore, 2 Science Drive 3, Singapore 117542

(Received 24 November 2016; published xxxxxx)

We demonstrate 17.7(1)% extinction of a weak coherent field by a single atom. We observe a shift of the resonance frequency and a decrease in interaction strength with the external field when the atom, initially at 21(1)  $\mu$ K, is heated by the recoil of the scattered photons. Comparing to a simple model, we conclude that the initial temperature reduces the interaction strength by less than 10%.

DOI: [10.1103/PhysRevA.00.003800](https://doi.org/10.1103/PhysRevA.00.003800)

### I. INTRODUCTION

The prospects of distributed quantum networks have triggered much effort in developing interfaces between single photons and single atoms (or other quantum emitters) [1]. A major challenge lies in increasing the interaction strength of the atom with incoming photons, which is a key ingredient for efficient transfer of quantum information from photons to atoms. While cavity-QED experiments have made tremendous progress in this direction [2,3], it remains an open question whether (near-)deterministic absorption of single photons is also possible without a cavity [4–7].

Single trapped atoms are a particularly good experimental platform for quantitative comparisons of light-matter experiments with quantum optics theory. The clean energy level structure and the trapping in ultrahigh vacuum permits deriving the interaction strength with a minimum of assumptions. In a free-space light-atom interface (as opposed to a situation with light fields in cavities with a discrete mode spectrum), the interaction strength is characterized by a single parameter, the spatial mode overlap  $\Lambda \in [0, 1]$ , which quantifies the similarity of the incident light field to the atomic dipole mode [8,9]. The development of focusing schemes with large spatial mode overlap is a longstanding theoretical [10–14] and experimental [4,15–23] challenge. Approaches with multielement objectives [4,16,17,23], singlet [18,24] and Fresnel lenses [25], and parabolic mirrors [26,27] have been used with various single-emitter systems. However, the interaction strengths observed with these configurations [13,22] have fallen short of their theoretically expected capabilities. Consequently, a better understanding of the underlying reasons is necessary to further improve the interaction strength. Aside from imperfections of the focusing devices, the finite positional spread of the single atomic emitter is commonly suspected to reduce the interaction [28].

In this paper, we present a light-atom interface based on a high numerical aperture lens and quantify the effect of insufficient localization of the atom on the light-atom interaction. Initially at sub-Doppler temperatures, we heat the atom in a well-controlled manner by scattering near-resonant photons and obtain a temperature dependency of the interaction strength and resonance frequency.

This paper is organized as follows. In Sec. II, we describe the optical setup and the measurement sequence. We then char-

acterize the light-atom interaction strength by a transmission (Sec. III) and a reflection (Sec. IV) measurement and present the dependence of the light-atom interaction on the positional spread of the atom in Sec. V.

### II. EXPERIMENTAL SETUP AND MEASUREMENT SEQUENCE

The core of the optical setup is a pair of high numerical aperture lenses  $L_1$  and  $L_2$  (NA = 0.75, focal length  $f = 5.95$  mm; see Fig. 1). A single <sup>87</sup>Rb atom is trapped at the joint focus of these lenses with a far-off-resonant, red-detuned optical dipole trap (852 nm) [29,30]. The circularly polarized ( $\sigma^+$ ) trap has a depth of  $U_0 = k_B \times 2.22(1)$  mK, with measured radial frequencies  $\omega_x/2\pi = 107(1)$  kHz and  $\omega_y/2\pi = 124(1)$  kHz, and an axial frequency  $\omega_z/2\pi = 13.8(1)$  kHz.

We probe the light-atom interaction by driving the closed transition  $5S_{1/2}, F=2, m_F = -2$  to  $5P_{3/2}, F=3, m_F = -3$  near 780 nm. The spatial mode of the incident probe field is defined by the aperture of the single-mode fiber, the collimation lens  $C_1$ , and the focusing lens  $L_1$ . The beam profile before  $L_1$  is approximately Gaussian, with a waist  $w_L = 2.7$  mm. Following [13,31], the spatial mode overlap  $\Lambda$  of the circularly polarized Gaussian mode focused by an ideal lens with the dipole mode of a stationary atom depends on the focusing strength  $u := w_L/f$ ,

$$\Lambda = \frac{3}{16u^3} e^{2/u^2} \left[ \Gamma\left(-\frac{1}{4}, \frac{1}{u^2}\right) + u \Gamma\left(\frac{1}{4}, \frac{1}{u^2}\right) \right]^2, \quad (1)$$

where  $\Gamma(a, b)$  is the incomplete gamma function. For our experimental parameters, we expect  $\Lambda = 11.2\%$ .

The experimental sequence used in Secs. III–V is depicted in Fig. 2. After loading a single atom into the dipole trap, the atom is cooled by polarization gradient cooling (PGC) [32]. For efficient cooling, we apply an additional  $\sigma^-$ -polarized dipole field (852 nm) injected through the same optical fiber as the  $\sigma^+$ -polarized dipole field. The  $\sigma^-$ -polarized dipole field, which is switched off after the PGC interval, originates from an independent laser running several hundreds of GHz detuned from the  $\sigma^+$ -polarized dipole field. Subsequently, a bias magnetic field of 0.74 mT is applied along the optical axis, and the atom is prepared in the  $5S_{1/2}, F=2, m_F = -2$  state by optical pumping. Next, the probe field is switched on for a duration  $t_p$  during which the detection events at avalanche photodetectors (APD)  $D_b$  and  $D_f$  are recorded. Finally, we perform a reference measurement to determine the power of

\*christian.kurtsiefer@gmail.com

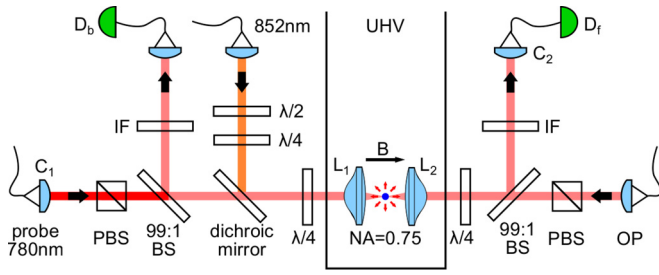


FIG. 1. Setup for probing light-atom interaction in free space. D: detector; UHV: ultrahigh vacuum chamber; IF: interference filter centered at 780 nm;  $\lambda/2$ : half-wave plate;  $\lambda/4$ : quarter-wave plate; C: fiber coupling lens; PBS: polarizing beam splitter; BS: beam splitter; L: high numerical aperture lens; B: magnetic field; OP: optical pumping.

the probe pulse. Optically pumping to the  $5S_{1/2}, F=1$  hyperfine state shifts the atom out of resonance with the probe field by 6.8 GHz. The probe pulse is reapplied for a time  $t_p$ , and we infer the average number of incident probe photons at the position of the atom from counts at detector  $D_f$  during the reference pulse, taking into account the optical losses from the position of the atom to detector  $D_f$ .

We determine the detection efficiencies of  $D_b$  and  $D_f$  by comparing against a calibrated pin photodiode and a calibrated APD to  $\eta_b = 59(3)\%$  and  $\eta_f = 56(4)\%$ , respectively. The experimental detection rates presented in the following are background corrected for 300 cps at detector  $D_b$  and 155 cps at detector  $D_f$ .

### III. EXTINCTION MEASUREMENT

In this section, we describe an extinction measurement to determine the spatial mode overlap  $\Lambda$  between probe and atomic dipole mode. For this, we compare the transmitted power through the system during the probe and the reference interval. To detect the transmitted power, the probe mode is recollimated by the second aspheric lens  $L_2$  and then coupled into a single-mode fiber directing the light to the forward detector  $D_f$ . The total electric field  $\vec{E}'(\vec{r})$  of the light moving away from the atom is a superposition of the probe field  $\vec{E}_p(\vec{r})$  and the field scattered by the atom  $\vec{E}_{sc}(\vec{r})$ :

$$\vec{E}'(\vec{r}) = \vec{E}_p(\vec{r}) + \vec{E}_{sc}(\vec{r}). \quad (2)$$

The electric field amplitude  $E_f = \int \vec{E}'(\vec{r})G^*(\vec{r})dS$  at the detector  $D_f$  is given by the spatial mode overlap of the total

	15ms	5ms	$t_p$	5ms	$t_p$
polarization gradient cooling	█				
$\sigma^+$ polarization dipole field	█	█	█	█	█
$\sigma$ polarization dipole field	█				
magnetic field		█	█	█	█
optical pumping to $F=2, m_f=-2$		█			
optical pumping to $F=1$				█	
probe field			█		█

FIG. 2. Experimental sequence to probe the light-atom interaction.

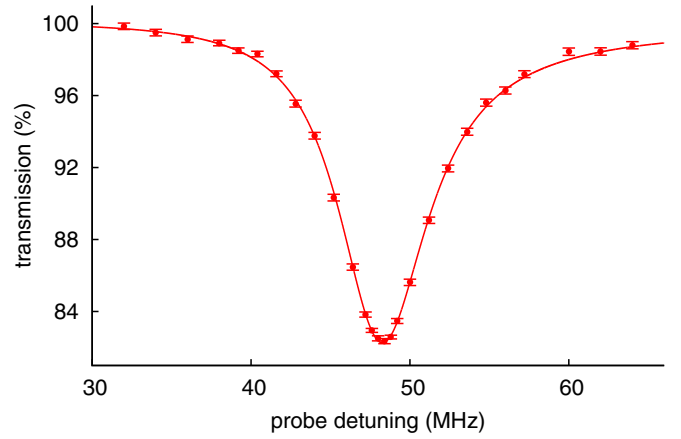


FIG. 3. Transmission measurement of a weak coherent probe beam. The solid line is a fit of Eq. (3) with free parameters: linewidth  $\Gamma/2\pi = 6.9(1)$  MHz, frequency shift  $\delta\omega = 48.03(3)$  MHz, spatial overlap  $\Lambda = 4.67(2)\%$ , and phase  $\phi_0 = 0.13(1)$  rad ( $\chi_{\text{red}}^2 = 1.01$ ), resulting in a resonant extinction of  $\epsilon = 17.7(1)\%$ . Error bars represent one standard deviation due to propagated Poissonian counting uncertainties.

electric field with the collection mode  $G(\vec{r})$  ( $dS$  is a differential area element perpendicular to the optical axis) [20]. In this configuration,  $\Lambda$  cannot be deduced from the transmitted power without knowledge or assumptions about this mode overlap [15–19,33]. The relative transmission  $\tau(\omega_p)$ , which is the optical power at detector  $D_f$  normalized to the reference power, contains Lorentzian and dispersionlike terms [17],

$$\tau(\omega_p) = 1 + A^2 \mathcal{L}(\omega_p) + 2A \mathcal{L}(\omega_p) \times \left[ (\omega_p - \omega_0 - \delta\omega) \sin \phi - \frac{\Gamma}{2} \cos \phi \right], \quad (3)$$

where  $\mathcal{L}(\omega_p) = 1/[(\omega_p - \omega_0 - \delta\omega)^2 + \Gamma^2/4]$  is a Lorentzian profile with linewidth  $\Gamma$ ,  $\omega_p$  is the frequency of the probe field, and coefficient  $A$  and the phase  $\phi$  depend on the mode matching of the probe and the collection mode. The resonance frequency shift  $\delta\omega = \omega_z + \omega_{ac}$  from the natural transition frequency  $\omega_0$  is due to a Zeeman shift  $\omega_z$  and an ac Stark shift  $\omega_{ac}$ . For perfect mode matching (e.g., when the collimation lens is identical to the focusing lens), the coefficients in Eq. (3) simplify to  $A = \Gamma\Lambda$  and  $\phi = 0$ . The transmission spectrum takes a purely Lorentzian form with a resonant extinction  $\epsilon = 4\Lambda(1 - \Lambda)$  [20].

We measure the transmission of a weak probe field for  $t_p = 20$  ms containing on average 550 photons per pulse. Tuning the frequency of the probe field, we find a maximum extinction  $\epsilon = 17.7(1)\%$  (Fig. 3). The observed transmission spectrum shows a small deviation from a Lorentzian profile. This deviation is caused by the imperfect mode overlap between probe and collection mode. We infer a mode overlap of approximately 70% from the probe power measured at detector  $D_f$ , corrected for losses of the optical elements. To account for the small deviation from the ideal case, we include the phase  $\phi$  as a free fit parameter. The model in Eq. (3) fits the observed values with four free parameters ( $\chi_{\text{red}}^2 = 1.01$ ): frequency shift  $\delta\omega = 48.03(3)$  MHz, spatial overlap  $\Lambda = 4.67(2)\%$ , phase  $\phi_0 = 0.13(1)$  rad, and linewidth  $\Gamma/2\pi = 6.9(1)$  MHz (slightly

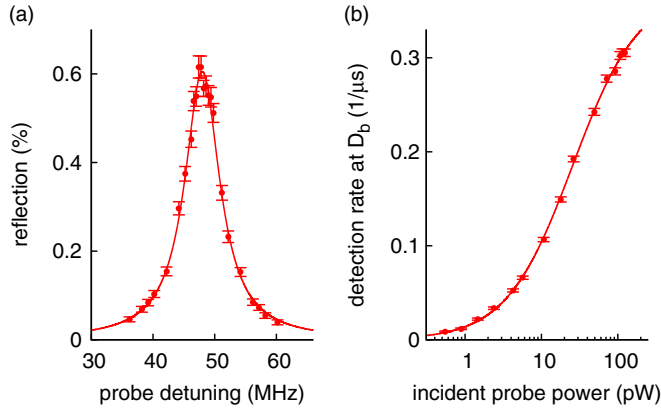


FIG. 4. (a) Light scattered into the backward detector  $D_b$  for different probe detunings. The solid line is a Lorentzian fit of Eq. (4) with free parameters linewidth  $\Gamma/2\pi = 6.9(1)$  MHz, frequency shift  $\delta\omega/2\pi = 48.0(1)$  MHz, and resonant backscattering probability  $P_{b,0} = 0.61(1)\%$ , with  $\chi_{\text{red}}^2 = 1.03$ . (b) Resonant saturation measurement, with the solid line representing the fit of Eq. (6) with saturation power  $P_{\text{sat}} = 26(2)$  pW and total detection efficiency  $\eta = 1.95(2)\%$  as free parameters ( $\chi_{\text{red}}^2 = 1.3$ ). Error bars represent one standard deviation due to propagated Poissonian counting uncertainties.

broader than the natural linewidth  $\Gamma_0/2\pi = 6.07$  MHz [34]. This interaction strength is 50% larger compared to our previous experiments with lenses of smaller numerical aperture (NA = 0.55 [18]).

#### IV. SATURATION MEASUREMENT

We also determine  $\Lambda$  from the intensity of the atomic fluorescence at backward detector  $D_b$ . Figure 4(a) shows the probability  $P_b$  for an incident photon to be backscattered by the atom when tuning the frequency  $\omega_p$  of the probe field. This value is obtained by normalizing the number of detected photons at detector  $D_b$  to the average number of incident photons during the probe interval  $t_p = 20 \mu\text{s}$  [35,36]. The backscattering probability is proportional to the atomic excited-state population and therefore follows a Lorentzian profile,

$$P_b = \frac{P_{b,0}}{4(\omega_p - \omega_0 - \delta\omega)^2/\Gamma^2 + 1}, \quad (4)$$

where  $P_{b,0}$  is the resonant backscattering probability. The experimental values of  $P_b$  in Fig. 4 can be well described by this model, with a frequency shift  $\delta\omega/2\pi = 48.0(1)$  MHz from the natural transition frequency,  $P_{b,0} = 0.61(1)\%$ , and  $\Gamma/2\pi = 6.9(1)$  MHz.

The incident power needed to saturate the target transition is a direct measurement of  $\Lambda$ . For a resonantly driven two-level atom, the saturation power  $P_{\text{sat}}$  is given by

$$P_{\text{sat}} = \frac{\hbar\omega_0\Gamma_0}{8} \frac{1}{\Lambda}, \quad (5)$$

where  $\omega_0$  is the transition frequency [22]. For complete mode matching ( $\Lambda = 1$ ), Eq. (5) gives a saturation power  $P_{\text{sat},\Lambda=1} = 1.21$  pW for the considered transition. The spatial overlap  $\Lambda = P_{\text{sat}}/P_{\text{sat},\Lambda=1}$  is obtained from the experimentally determined saturation power  $P_{\text{sat}}$ .

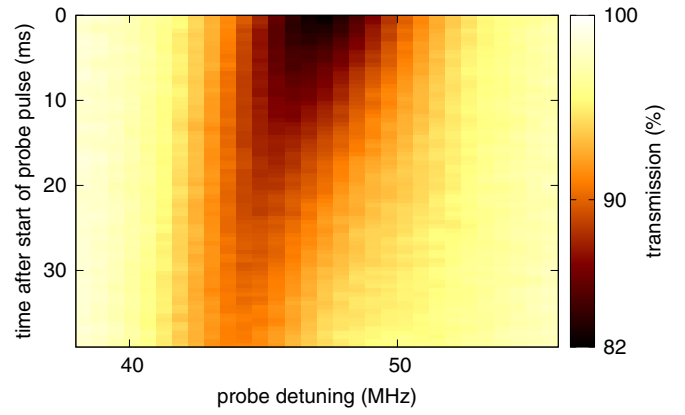


FIG. 5. Time-resolved extinction measurement. Each row presents a transmission spectrum similar to Fig. 3 and is obtained by collecting photodetection events in 0.5-ms-wide time bins. As the atom is heated by scattering probe photons, the transmission increases and the frequency of the minimal transmission shifts to a lower detuning from the unperturbed resonance.

The saturation power  $P_{\text{sat}}$  is determined by varying the excitation power on resonance [see Fig. 4(b)]. We use a short probe interval ( $t_p = 4 \mu\text{s}$ ) to minimize heating of the atom. A saturation power of  $P_{\text{sat}} = 26(2)$  pW and a total detection efficiency  $\eta = 1.95(2)\%$  are obtained from fitting the resultant atomic fluorescence rate  $R_b$  to the expected saturation function,

$$R_b = \frac{\eta\Gamma_0}{2} \frac{P_{\text{inc}}}{P_{\text{inc}} + P_{\text{sat}}}, \quad (6)$$

where  $P_{\text{inc}}$  is the power of the incident beam at the position of the atom. We infer a total collection efficiency  $\eta_{\text{sm}} = \eta/\eta_b = 3.3(3)\%$  into a single-mode fiber, which is compatible with the highest efficiencies reported for a free-space optic [37,38]. Comparing  $P_{\text{sat}}$  to  $P_{\text{sat},\Lambda=1}$  indicates a spatial overlap  $\Lambda = 4.7(4)\%$ , in agreement with the extinction measurement  $\Lambda = 4.67(2)\%$ . The uncertainty of the spatial overlap is dominated by the uncertainty of the efficiency  $\eta_f$  of detector  $D_f$ , which we use in conjunction with a set of calibrated neutral density filters to determine the incident power  $P_{\text{inc}}$ .

#### V. TEMPERATURE DEPENDENCE OF LIGHT-ATOM INTERACTION

We investigate whether the residual temperature of the atom limits the coupling to the probe field. As the recoil associated with the scattering of the probe field increases the kinetic energy of the atom, different atom temperatures can be accessed by following the temporal evolution of the probe transmission. The photodetection events during the probe interval are time tagged and sorted into 0.5-ms-wide time bins, resulting in the time-resolved transmission spectrum shown in Fig. 5. The probe pulse has a length of  $t_p = 40$  ms and contains, on average, about 9000 photons. As the probe pulse progresses, the resonance frequency shifts towards lower frequencies and the extinction reduces.

Extracting the temperature dependency of the light-atom interaction directly from the time-resolved transmission spectrum (Fig. 5) is difficult because the scattering rate and

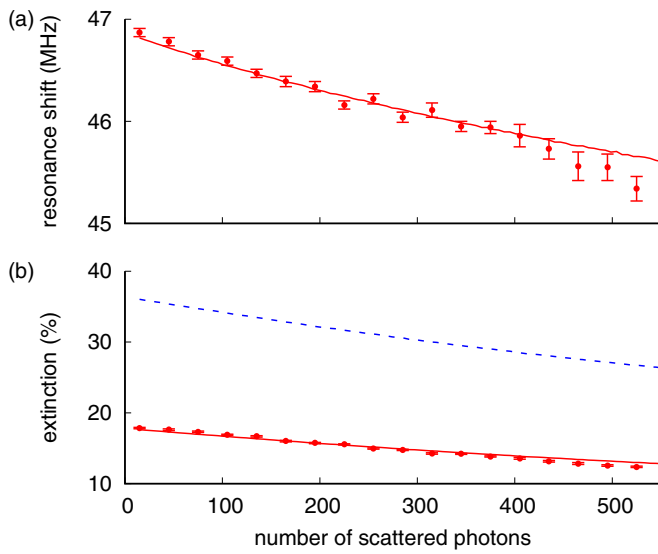


FIG. 6. The effect of recoil heating on the (a) resonance frequency and (b) extinction obtained by rearranging the histogram in Fig. 5 with a bin width of 30 scattered photons. Resonance frequency and extinction decrease fairly linearly as the atom heats up. (a) Solid red line is the numerical result of Eq. (8) with the frequency shift at the center of trap  $\delta\omega(0)$  as a free fit parameter ( $\chi_{\text{red}}^2 = 1.4$ ). (b) The temperature dependence is well reproduced by Eq. (8) with  $\alpha = 0.54(1)$  as a free fit parameter (red solid line,  $\chi_{\text{red}}^2 = 11.6$ ). The dashed blue line is the expected extinction for an ideal lens, given by Eq. (8), with  $\alpha = 0$ . Error bars represent one standard deviation obtained from the least-squares fit of the individual spectra.

therefore the motional heating vary during the probe interval and depend on the probe frequency. For a quantitative analysis, we sort the detection events for each probe frequency according to the number of scattered photons instead of the probe pulse duration  $t_p$ . The number of scattered photons,  $n_s(t)$ , time integrated from the beginning of the probe interval to time  $t$ , is calculated from the transmitted photons via

$$n_s(t) = \sum_{t_i=0}^t [n_{\text{ref}}(t_i) - n_p(t_i)] / \eta_f \eta_{\text{op}}, \quad (7)$$

where  $n_{\text{ref}}(t_i)$  and  $n_p(t_i)$  are the numbers of detected photons at detector  $D_f$  in time bin  $t_i$  during the reference and the probe interval, respectively,  $\eta_{\text{op}} = 59(5)\%$  is the optical loss from the atom to the detector, and  $\eta_f$  is the detection efficiency. We choose a relative bin width of 30 scattered photons and obtain the resonance frequency and the extinction by fitting to Eq. (3). The resonance frequency and the extinction decrease fairly linearly with the number of scattered photons (Fig. 6). After scattering approximately 500 photons, the resonance frequency is lowered by 1.5(1) MHz and the extinction is reduced by approximately 30% to  $\epsilon = 12.4(1)\%$ .

We derive the temperature-dependent transmission spectrum by including the spatial dependence of the frequency shift  $\delta\omega(\vec{r}) = \omega_z + \omega_{\text{ac}}(\vec{r})$  and the mode overlap  $\Lambda(\vec{r})$  [39] in Eq. (3), where  $\vec{r}$  is the position of the atom relative to the center of the trap. The ac Stark shift  $\omega_{\text{ac}}(\vec{r})$  is treated in the paraxial approximation, given the large beam waist of 1.4  $\mu\text{m}$  of the dipole trap. For the probe field, we use the effective interaction

strength  $\Lambda_{\text{eff}}(\vec{r}) = (1 - \alpha)\Lambda(\vec{r})$ , where we evaluate the spatial dependence of the mode overlap  $\Lambda(\vec{r})$  according to [13], which includes the changes of the local electric field polarization of the probe light near the focus. In addition, we heuristically introduce the parameter  $\alpha$  which accounts for a reduced interaction strength due to experimental imperfections. The transmission spectrum, averaged over many different spatial configurations, is then given by

$$\langle \tau \rangle = \int p(T, \vec{r}) \tau(\vec{r}) d^3r, \quad (8)$$

where  $p(T, \vec{r})$  is the probability distribution of the atom position. We treat the motion of the atom classically and assume that the probability distribution  $p(T, \vec{r})$  is governed by a Maxwell-Boltzmann distribution with standard deviations of the positional spread of the atom  $\sigma_i = \sqrt{k_B T / m \omega_i^2}$ , with  $i = x, y, z$  and mass  $m$  of  $^{87}\text{Rb}$ . Equation (8) can then be evaluated by a Monte Carlo method. Each scattered photon increases the total energy of the atom by  $2E_r$ , where  $E_r = \hbar^2 k^2 / 2m$  is the photon recoil energy. The gained energy is anisotropically distributed because of the unidirectional excitation by the probe beam. Each photon leads therefore, on average, to an energy increase of  $\frac{2}{3}E_r$  in the radial directions and  $\frac{4}{3}E_r$  in the axial direction. From a release-recapture technique [40], we infer an initial atom temperature of 21(1)  $\mu\text{K}$ . Thus, after 500 scattering events, the axial temperature is increased by approximately 120  $\mu\text{K}$  to just below Doppler temperature,  $T_D = 146 \mu\text{K}$ .

The frequency shift expected from Eq. (8) matches well with the experimental results [Fig. 6(a)], where we use only the frequency shift at the center of the trap  $\delta\omega(0) = 47.32(5)$  MHz as a free fit parameter. This good agreement indicates that the model captures the effect of the dipole trap well. The initial resonance frequency is slightly lower compared to the results in Secs. IV and III because of a slightly lower dipole trap power. Figure 6(b) (solid red line) shows the theoretical extinction expected from Eq. (8) with our focusing parameters using  $\alpha = 54(1)$  as a free parameter. The reduction of the extinction as a function of scattered photons is well reproduced by the model. From Eq. (8) with  $\alpha = 0.54(1)$ , we extrapolate a spatial overlap  $\Lambda = 5.1\%$  for a stationary atom which is approximately 10% larger than the interaction observed for our lowest temperatures. This estimation provides an upper bound for the temperature effect because our model treats the atomic motion classically and therefore does not include the finite spread of the motional ground state. The large value of  $\alpha = 0.54(1)$  means we observe less interaction compared to the tight focusing theory outlined in [13]. This reduction is likely to be caused by imperfections of the focusing lens and deviations of the incident field from a Gaussian beam.

Finally, we discuss possible origins of the observed linewidth broadening (Figs. 3 and 4). Doppler and power broadening are negligible because of the low atomic temperature of 21(1)  $\mu\text{K}$  and the weak excitation field in both measurements,  $P_{\text{probe}} < 0.02 P_{\text{sat}}$ . We use Eq. (8) to estimate whether the broadening is caused by the thermal motion in the spatially varying trap potential. We find an expected linewidth of 6.3 MHz for  $T = 21 \mu\text{K}$ . Therefore, we attribute

295 the residual linewidth broadening to other noise sources, such  
 296 as the linewidth of the probe laser.

297 **VI. CONCLUSION**

298 We demonstrated an effective spatial mode overlap  $\Lambda =$   
 299  $4.7(4)\%$  between an external probe mode and the atomic  
 300 dipole mode, and showed that the light-atom interaction can be  
 301 limited by the residual motion of the atom even at sub-Doppler  
 302 temperatures. The spatially varying ac Stark shift and the  
 303 tight confinement of the probe field cause a reduction of  
 304 approximately 10% in interaction strength for our lowest  
 305 atom temperatures. Thus, cooling to the motional ground  
 306 state promises only a moderate improvement [41,42]. Further

improvement of the interaction strength requires a more careful 307  
 analysis of the focusing lens and the application of aberration 308  
 corrections to the incident probe field. In addition, coherent 309  
 control of the atomic motion and temporal shaping of the 310  
 incoming photon can optimize the absorption efficiency [6,43]. 311

312 **ACKNOWLEDGMENTS**

We thank V. Leong and N. Lewty for contributions in an 313  
 early stage of the experiment. We acknowledge the support 314  
 of this work by the Ministry of Education in Singapore 315  
 (AcRF Tier 1) and the **National Research Foundation, Prime** 316  
**Minister's office**. M.S. acknowledges financial support by the 317  
 Lee Kuan Yew Postdoctoral Fellowship. 318

---

[1] H. J. Kimble, *Nature (London)* **453**, 1023 (2008).  
 [2] J. Volz, R. Gehr, G. Dubois, J. Esteve, and J. Reichel, *Nature (London)* **475**, 210 (2011).  
 [3] A. Reiserer, S. Ritter, and G. Rempe, *Science* **342**, 1349 (2013).  
 [4] N. Piro, F. Rohde, C. Schuck, M. Almendros, J. Huwer, J. Ghosh, A. Haase, M. Hennrich, F. Dubin, and J. Eschner, *Nat. Phys.* **7**, 17 (2011).  
 [5] Y. L. A. Rezus, S. G. Walt, R. Lettow, A. Renn, G. Zumofen, S. Götzinger, and V. Sandoghdar, *Phys. Rev. Lett.* **108**, 093601 (2012).  
 [6] V. Leong, M. A. Seidler, M. Steiner, A. Cerè, and C. Kurtsiefer, *Nat. Commun.* **7**, 13716 (2016).  
 [7] J. Brito, S. Kucera, P. Eich, P. Müller, and J. Eschner, *Appl. Phys. B* **122**, 1 (2016).  
 [8] A. Golla, B. Chalopin, M. Bader, I. Harder, K. Mantel, R. Maiwald, N. Lindlein, M. Sondermann, and G. Leuchs, *Eur. Phys. J. D* **66**, 1 (2012).  
 [9] G. Leuchs and M. Sondermann, *J. Mod. Opt.* **60**, 36 (2013).  
 [10] S. J. van Enk and H. J. Kimble, *Phys. Rev. A* **61**, 051802 (2000).  
 [11] S. J. van Enk, *Phys. Rev. A* **69**, 043813 (2004).  
 [12] M. Sondermann, R. Maiwald, H. Konermann, N. Lindlein, U. Peschel, and G. Leuchs, *Appl. Phys. B* **89**, 489 (2007).  
 [13] M. K. Tey, G. Maslennikov, T. C. H. Liew, S. A. Aljunid, F. Huber, B. Chng, Z. Chen, V. Scarani, and C. Kurtsiefer, *New J. Phys.* **11**, 043011 (2009).  
 [14] G. Hétet, L. Slodička, A. Glätzle, M. Hennrich, and R. Blatt, *Phys. Rev. A* **82**, 063812 (2010).  
 [15] D. J. Wineland, W. M. Itano, and J. C. Bergquist, *Opt. Lett.* **12**, 389 (1987).  
 [16] A. N. Vamivakas, M. Atatüre, J. Dreiser, S. T. Yilmaz, A. Badolato, A. K. Swan, B. B. Goldberg, A. Imamoglu, and M. S. Ünlü, *Nano Lett.* **7**, 2892 (2007).  
 [17] I. Gerhardt, G. Wrigge, P. Bushev, G. Zumofen, M. Agio, R. Pfab, and V. Sandoghdar, *Phys. Rev. Lett.* **98**, 033601 (2007).  
 [18] M. K. Tey, Z. Chen, S. A. Aljunid, B. Chng, F. Huber, G. Maslennikov, and C. Kurtsiefer, *Nat. Phys.* **4**, 924 (2008).  
 [19] G. Wrigge, I. Gerhardt, J. Hwang, G. Zumofen, and V. Sandoghdar, *Nat. Phys.* **4**, 60 (2008).  
 [20] S. A. Aljunid, M. K. Tey, B. Chng, T. Liew, G. Maslennikov, V. Scarani, and C. Kurtsiefer, *Phys. Rev. Lett.* **103**, 153601 (2009).  
 [21] M. Pototschnig, Y. Chassagneux, J. Hwang, G. Zumofen, A. Renn, and V. Sandoghdar, *Phys. Rev. Lett.* **107**, 063001 (2011).  
 [22] M. Fischer, M. Bader, R. Maiwald, A. Golla, M. Sondermann, and G. Leuchs, *Appl. Phys. B* **117**, 797 (2014).  
 [23] T. H. Tran, J. Wrachtrup, and I. Gerhardt, *arXiv:1608.05224*. 1  
 [24] Y. R. P. Sortais, H. Marion, C. Tuchendler, A. M. Lance, M. Lamare, P. Fournet, C. Armellin, R. Mercier, G. Messin, A. Browaeys, and P. Grangier, *Phys. Rev. A* **75**, 013406 (2007).  
 [25] E. W. Streed, B. G. Norton, A. Jechow, T. J. Weinhold, and D. Kielpinski, *Phys. Rev. Lett.* **106**, 010502 (2011).  
 [26] R. Maiwald, A. Golla, M. Fischer, M. Bader, S. Heugel, B. Chalopin, M. Sondermann, and G. Leuchs, *Phys. Rev. A* **86**, 043431 (2012).  
 [27] L. Alber, M. Fischer, M. Bader, K. Mantel, M. Sondermann, and G. Leuchs, *arXiv:1609.06884*.  
 [28] G. R. Guthohrlein, M. Keller, K. Hayasaka, W. Lange, and H. Walther, *Nature (London)* **414**, 49 (2001).  
 [29] N. Schlosser, G. Reymond, I. Protsenko, and P. Grangier, *Nature (London)* **411**, 1024 (2001).  
 [30] N. Schlosser, G. Reymond, and P. Grangier, *Phys. Rev. Lett.* **89**, 023005 (2002).  
 [31] S. A. Aljunid, G. Maslennikov, Y. Wang, H. L. Dao, V. Scarani, and C. Kurtsiefer, *Phys. Rev. Lett.* **111**, 103001 (2013).  
 [32] P. D. Lett, R. N. Watts, C. I. Westbrook, W. D. Phillips, P. L. Gould, and H. J. Metcalf, *Phys. Rev. Lett.* **61**, 169 (1988).  
 [33] J. Hwang and W. Moerner, *Opt. Commun.* **280**, 487 (2007).  
 [34] U. Volz and H. Schmoranzler, *Phys. Scr.* **1996**, 48 (1996).  
 [35] S. A. Aljunid, B. Chng, J. Lee, M. Paesold, G. Maslennikov, and C. Kurtsiefer, *J. Mod. Opt.* **58**, 299 (2011).  
 [36] G. Zumofen, N. M. Mojarad, V. Sandoghdar, and M. Agio, *Phys. Rev. Lett.* **101**, 180404 (2008).  
 [37] D. Hucul, I. V. Inlek, G. Vittorini, C. Crocker, S. Debnath, S. M. Clark, and C. Monroe, *Nat. Phys.* **11**, 37 (2015).  
 [38] M. Ghadimi, V. Blums, B. G. Norton, P. M. Fisher, S. C. Connell, J. M. Amini, C. Volin, H. Hayden, C. S. Pai, D. Kielpinski, M. Lobino, and E. Streed, *Quantum Inf.* **3**, 4 (2016). 2  
 [39] C. Teo and V. Scarani, *Opt. Commun.* **284**, 4485 (2011).  
 [40] C. Tuchendler, A. M. Lance, A. Browaeys, Y. R. P. Sortais, and P. Grangier, *Phys. Rev. A* **78**, 033425 (2008).  
 [41] A. M. Kaufman, B. J. Lester, and C. A. Regal, *Phys. Rev. X* **2**, 041014 (2012).  
 [42] J. D. Thompson, T. G. Tiecke, A. S. Zibrov, V. Vuletić, and M. D. Lukin, *Phys. Rev. Lett.* **110**, 133001 (2013).  
 [43] N. Trautmann, G. Alber, and G. Leuchs, *Phys. Rev. A* **94**, 033832 (2016).